CLIMATOLOGY

The tropical lapse rate steepened during the Last Glacial Maximum

Shannon E. Loomis,[1] James M. Russell,[1,2]* Dirk Verschuren,[3] Carrie Morrill,[4,5] Gijs De Cort,[3,6] Jaap S. Sinninghe Damsté,[7,8] Daniel Olago,[9,10] Hilde Eggermont,[3,11] F. Alayne Street-Perrott,[12] Meredith A. Kelly[13]

2017 © The Authors, some rights reserved; exclusive licensee American Association for the Advancement of Science. Distributed under a Creative Commons Attribution NonCommercial License 4.0 (CC BY-NC).

The gradient of air temperature with elevation (the temperature lapse rate) in the tropics is predicted to become less steep during the coming century as surface temperature rises, enhancing the threat of warming in high-mountain environments. However, the sensitivity of the lapse rate to climate change is uncertain because of poor constraints on high-elevation temperature during past climate states. We present a 25,000-year temperature reconstruction from Mount Kenya, East Africa, which demonstrates that cooling during the Last Glacial Maximum was amplified with elevation and hence that the lapse rate was significantly steeper than today. Comparison of our data with paleoclimate simulations indicates that state-of-the-art models underestimate this lapse-rate change. Consequently, future high-elevation tropical warming may be even greater than predicted.

Downloaded from http://advances.sciencemag.org/ on April 18, 2017

INTRODUCTION

Recent climate change in the world's high tropical mountains has caused widespread retreat of tropical glaciers (*1*) and stress to local economies reliant on mountain resources (*2*). In the coming century, these areas are predicted to experience a magnitude of warming second only to the Arctic due, in part, to amplification of warming with elevation in the tropics (*3*). Proxy data indicate that substantial changes in tropical temperature and mountain environments occurred during the last deglaciation, the most recent time period when rising atmospheric CO_2 concentrations were associated with great changes in temperature. Determining whether the lapse rate of temperature (hereafter the lapse rate) changed during this period could therefore have important implications for the future of tropical glaciers, the hydrological cycle, and some of the world's most economically vulnerable societies.

More than 30 years ago, the CLIMAP project (*4*) suggested that tropical sea surface temperatures (SSTs) cooled by only ~1°C, on average, during the peak of the last ice age [Last Glacial Maximum (LGM) between 26 and 19 thousand years ago (ka)]. Glaciological and climate modeling data available at that time showed that these small changes in tropical SSTs could not be reconciled with the much greater (5° to 10°C) LGM cooling estimated from the magnitude of snow line depression on tropical mountains (*5*), unless the lapse rate was much steeper than allowed by climate models (*6*). Many reasons have been proposed for this mismatch, from errors in reconstructed sea surface and continental temperatures to limitations in the parameterization and simulation of tropical convective processes (*7*–*9*). More recent syntheses of LGM SSTs indicate a mean tropical ocean surface cooling of ~2°C (*10*), slightly greater than the CLIMAP estimates, but paleovegetation and glacial moraine evidence has consistently suggested greater cooling on land and particularly at high elevation (*11*). Unfortunately, temperature inferences from these proxies can be biased by confounding influences from radiation, precipitation, humidity, cloudiness, atmospheric CO_2 concentration, and other environmental variables (*12*, *13*). Therefore, the most persistent obstacle to assessing the sensitivity of the lapse rate to climate change is correct quantification of past temperature changes in the high tropical troposphere.

The recent development of continental temperature proxies based on glycerol dialkyl glycerol tetraethers (GDGTs) provides a novel opportunity to quantitatively reconstruct past changes in the tropical lapse rate. GDGTs are membrane lipids synthesized by archaea and bacteria and are produced in East African lakes (*14*). Changes in the relative abundances of GDGTs containing different numbers of methyl branches and cyclopentane rings, quantified by the TEX_{86} and MBT/CBT indices for isoprenoidal and branched GDGTs (brGDGTs), respectively, correlate strongly to sea surface and surface air temperature (*15*). Here, we apply the brGDGT paleothermometer to the 25,000-year sediment record from Lake Rutundu, a maar lake at 3078 m above sea level (asl) on Mount Kenya in East Africa (see Fig. 1 and Materials and Methods). Long, continuous, quantitative temperature reconstructions at higher elevations are not possible because higher lakes formed during glacier recession after the LGM; thus, our reconstruction provides a unique combination of temporal length and elevation. We combine our record with earlier GDGT-based reconstructions from low- and mid-elevation sites to assess changes in the position of the 0°C isotherm [freezing-level height (FLH)], and consequently in the lapse rate, during the LGM (see Materials and Methods).

RESULTS

Our reconstruction indicates that the mean annual temperature at the elevation of Lake Rutundu was 5.5 ± 0.2°C cooler during the LGM than during the preindustrial (PI) period (that is, recent time before the onset of anthropogenic warming; Fig. 2A). After the LGM, temperature

[1]Department of Earth, Environmental, and Planetary Sciences, Brown University, 324 Brook Street, Box 1846, Providence, RI 02912, USA. [2]Institute at Brown for Environment and Society, Brown University, Providence, RI 02912, USA. [3]Department of Biology, Limnology Unit, Ghent University, K.L. Ledeganckstraat 35, 9000 Ghent, Belgium. [4]Cooperative Institute for Research in Environmental Sciences, University of Colorado at Boulder, Boulder, CO 80305–3328, USA. [5]National Centers for Environmental Information, National Oceanic and Atmospheric Administration, Boulder, CO 80305–3328 USA. [6]Department of Earth Sciences, Royal Museum for Central Africa, Leuvensesteenweg 13, 3080 Tervuren, Belgium. [7]Department of Marine Microbiology and Biogeochemistry, NIOZ Royal Netherlands Institute for Sea Research, P.O. Box 59, 1790 AB Den Burg, Texel, Netherlands. [8]Faculty of Geosciences, University of Utrecht, P.O. Box 80.021, 3508 TA Utrecht, Netherlands. [9]Department of Geology, University of Nairobi, P.O. Box 30197-00100, Nairobi, Kenya. [10]Institute for Climate Change and Adaptation, University of Nairobi, Nairobi, Kenya. [11]Belgian Biodiversity Platform, Royal Belgian Institute for Natural Sciences, Vautierstraat 29, 1000 Brussels, Belgium. [12]College of Science, Swansea University, Singleton Park, Swansea SA32 7QD, U.K. [13]Department of Earth Sciences, Dartmouth College, Hanover, NH 03750, USA.
*Corresponding author. Email: james_russell@brown.edu

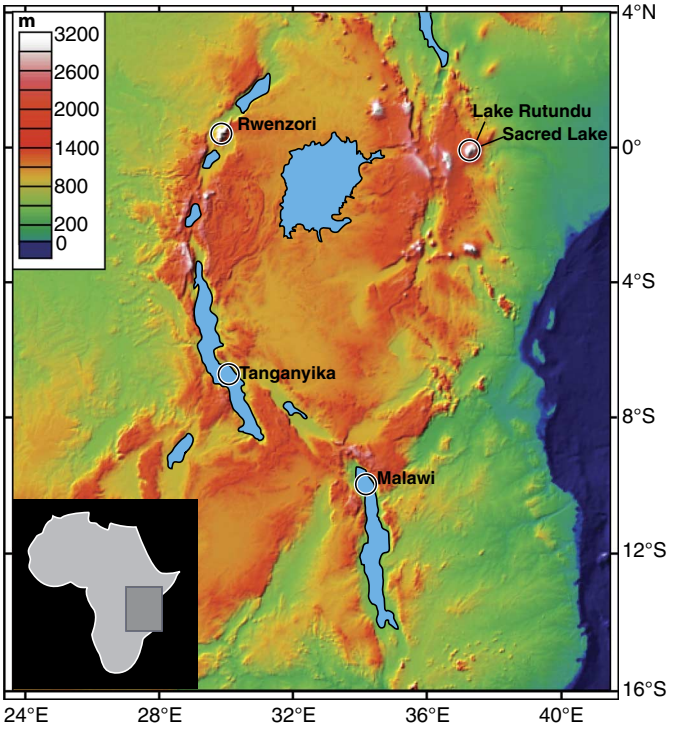

Fig. 1. Topographic map of eastern Africa. The locations of Lake Rutundu, Mount Kenya (0°03′S, 37°28′E), Sacred Lake, Mount Kenya (0°03′N, 37°32′E), Lake Tanganyika (6°42′S, 29°50′E), Lake Malawi (10°16′S, 34°19′E), and the Rwenzori Mountains (0°23′N, 29°52′E) are indicated with circles.

declined slightly until 17 ka and then rose during the late glacial and early Holocene to reach a mid-Holocene maximum centered at 5 ka. Temperature has decreased by ~1.5°C since the mid-Holocene, possibly in response to declining Northern Hemisphere fall insolation (*16*). Deglacial warming at Lake Rutundu was interrupted by pronounced cooling from ~12.8 to 11.8 ka, roughly coincident with the Younger Dryas (YD) chronozone. Our record supports previous documentation of YD cooling at the East African Lakes Albert (*17*) and Malawi (*18*). However, other lake-based temperature records from the region indicate little or no cooling during this time (*19*, *20*), perhaps due to local reductions in wind-driven water-column mixing (*21*) that offset surface cooling. Given these site-specific differences, we focus here on features common to all East African GDGT records: an LGM cooler than the PI, maximum temperatures during the mid-Holocene (4 to 7 ka), and gradual cooling from the mid-Holocene to the present.

We calculate the magnitude of LGM cooling relative to the PI (ΔT_{LGM}) as the difference in average temperature between the last two millennia (0 to 2 ka) and the local LGM, which is defined by ^{10}Be dating of Rwenzori glacial moraines as the period 20.1 to 23.4 ka (*22*) and which lies within the broader window of strongest global LGM cooling. ΔT_{LGM} differs significantly between the four available GDGT-based records (Fig. 2), from 5.5°C at Lake Rutundu (3081 m asl) and 5.2°C at Sacred Lake [2350 m asl (*20*)] to 3.3°C at Lake Tanganyika [773 m asl (*19*)] and 2.0°C at Lake Malawi [474 m asl (*18*)]. The reconstructions from Lake Rutundu and Sacred Lake are based on brGDGTs, whereas the Lake Malawi and Tanganyika reconstructions are based on TEX_{86}; thus, small disparities between proxy calibration methods might explain some of the record differences. However, the TEX_{86}-derived low-elevation ΔT_{LGM} values broadly conform to estimates of 2° to 4°C cooling derived from low-elevation vegetation change (*11*, *23*). All the terrestrial records indicate stronger cooling than the western equatorial Indian Ocean SST temperature decrease of 1.7°C reconstructed from alkenones (*24*, *25*). Moreover, the magnitude of reconstructed LGM cooling increases with elevation between each pair of TEX_{86} and brGDGT-based records; that is, ΔT_{LGM} at Tanganyika exceeds that at Malawi, and ΔT_{LGM} at Rutundu exceeds that at Sacred Lake. The great geographic distances between these proxy records might be expected to introduce error into our estimates of the lapse-rate change. However, the tropical troposphere exhibits very small horizontal temperature variations because of weak Coriolis forces that would otherwise balance thermally driven pressure differences (*26*). The present-day lapse rate varies by ~0.25°C/km over our study sites, suggesting that this is not a great source of error in our reconstructions (see the Supplementary Materials). We conclude that the greatest LGM cooling occurred at the highest elevations, implying that the environmental lapse rate was steeper during the LGM than it is today.

To quantify the LGM lapse rate ($\Delta\Gamma_{LGM}$), we subtract ΔT_{LGM} from the modern instrumental temperature at each site and regress these values against their respective elevations after accounting for LGM sea- and lake-level changes (see Materials and Methods). We found that $\Delta\Gamma_{LGM}$ was −6.7 ± 0.3°C/km, which was significantly steeper than the modern East African lapse rate of −5.8 ± 0.1°C/km determined from instrumental and reanalysis data (see Fig. 3A and the Supplementary Materials). This estimate of ΔT_{LGM} is statistically robust, given both the high correlation (r^2 = 0.93) and the low root mean square error (RMSE = 0.7°C). Independent confirmation of our estimate is provided by evidence from glacial moraines, which suggests that the average equilibrium line altitude (ELA) of glaciers on East Africa's high mountains was depressed by 1040 ± 220 m (*27*). Extrapolating our $\Delta\Gamma_{LGM}$ to estimate the FLH at the equator, we find that FLH_{LGM} was 1090 ± 130 m lower than the PI, indistinguishable from the mean estimated change in the region's ELA (P = 0.99) (see Fig. 3B and the Supplementary Materials). The elevations of FLH and ELA can differ because local ELAs can be affected by multiple environmental variables influencing glacier mass balance, including precipitation, humidity, and other processes governing radiation and sublimation (*13*, *27*). However, strong coherence between the independent GDGT proxy and glacial ELA data sets lends credence to our new estimate and also supports the hypothesis that temperature was the dominant control on tropical alpine glacier fluctuations at this time scale (*22*).

DISCUSSION

The present-day lapse rate over East Africa (−5.8°C/km) is slightly steeper than a moist adiabat (−5.5°C/km), which represents the mean annual tropical lapse rate below ~5000-m elevation. Above 5000 m, the tropical lapse rate gradually steepens toward a dry adiabat (~−9.8°C/km) because of mid-elevation cloud condensation and downdrafts carrying dry air from the high troposphere toward the 5000-m level (*28*). It is possible that, during the LGM, high-elevation temperatures were lowered by a depression of the cloud condensation height. Although this might explain the lower temperatures observed at the elevation of tropical glaciers, it does not explain the consistent linear lapse rate we observe between 0 and ~3100 m asl in our records, or the excellent agreement between the GDGT-based temperature estimates and those estimated from past glacial extents.

Downloaded from http://advances.sciencemag.org/ on April 18, 2017

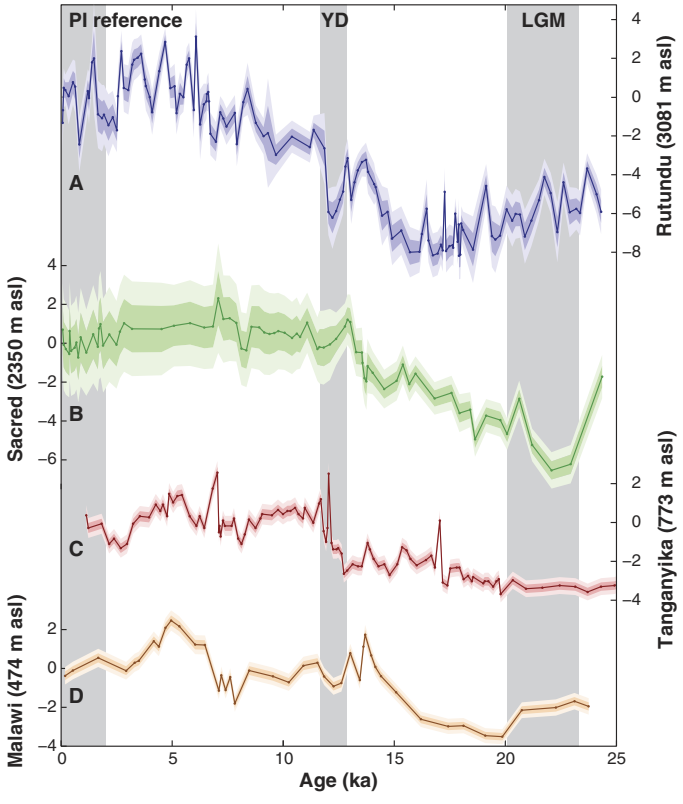

Fig. 2. Reconstructed time series of temperature change from the LGM to the present along an elevational gradient in tropical East Africa. (**A**) Lake Rutundu (data from this study, with two outliers removed). (**B**) Sacred Lake (*20*). (**C**) Lake Tanganyika (*19*). (**D**) Lake Malawi (*18*). Shading on the reconstructions denotes 68 and 95% confidence intervals (CIs) based on bootstrapping of the respective calibrations. Gray vertical shading denotes the age range of the regional LGM, defined by ^{10}Be ages of moraines from the Rwenzori Mountains, Uganda (*22*), the YD, and the PI reference interval used to calculate the lapse rate. The moraine ages are plotted in white boxes with 1σ error bars.

We argue that a steeper tropical lapse rate during the LGM developed because of a shift toward a dry adiabat in the lower troposphere. Atmospheric water vapor concentration in the tropics is largely controlled by global mean tropical temperature because of the temperature dependence of the saturation vapor pressure and the thermal homogeneity of the high tropical atmosphere (*29*). Although there are few proxies that record past atmospheric humidity, regional paleohydrological records demonstrate that most of East Africa was drier during the LGM than during the late Holocene (*30*). Moreover, despite significant regional temperature variations, such as the ~1.5°C mid-Holocene warming, our reconstructions reveal no significant change in the lapse rate during the globally warmer Holocene period, during which atmospheric humidity was likely more stable. Thus, our data suggest that the combination of global warming and rising humidity during the last deglaciation caused shoaling of the lapse rate.

Climate simulations for the LGM and the PI periods performed as part of the Coupled Model Intercomparison Project (CMIP5)/Paleoclimate Model Intercomparison Project 3 (PMIP3) produce a multi-model mean temperature change within the error of our reconstruction (Fig. 4A) at low-elevation sites (the western Indian Ocean and Lake Malawi; see Materials and Methods). CMIP5 models simulate a modern mean East African PI lapse rate of −6.0 ± 0.3°C/km, similar to observations, and a steeper (−6.4 ± 0.3°C/km) lapse rate during the LGM. However, the magnitude of simulated temperature change between the LGM and the PI at elevations above ~1000 m asl, such as at Lake Rutundu, is underestimated by up to 40% in the CMIP5 models, and the multi-model mean change in lapse rate (−0.4°C/km) is significantly lower ($P = 0.004$) than our reconstruction (−0.9°C/km). These results reinforce earlier data-model comparisons of the LGM lapse rate (*8*), indicating that, despite improvements of convection schemes and other model aspects in CMIP5, climate models continue to underestimate changes in high-elevation tropical temperature.

Although the difference between simulated and reconstructed lapse-rate change is significant, its causes are elusive. The lapse-rate changes simulated by the models are inversely correlated with changes in the specific ($P < 0.01$) and relative ($P < 0.02$) humidity of the mid to lower troposphere over East Africa, confirming that a drier LGM climate contributed to a steeper LGM lapse rate (see the Supplementary

Downloaded from http://advances.sciencemag.org/ on April 18, 2017

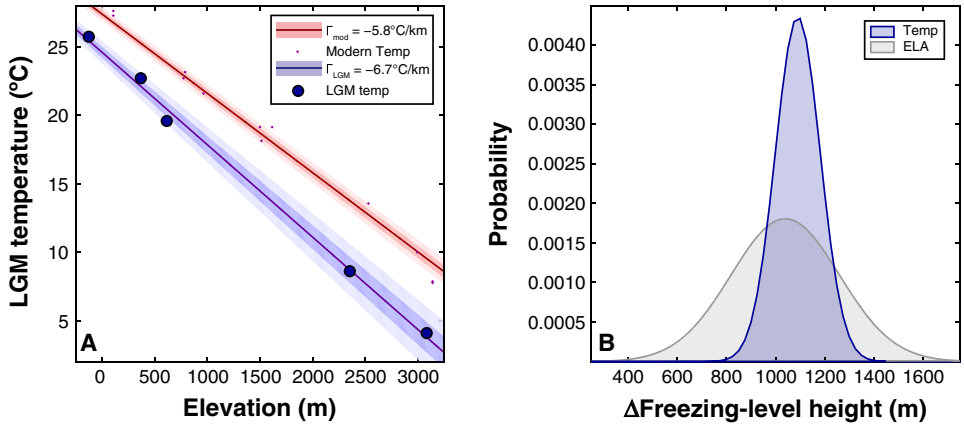

Fig. 3. Reconstructed changes in lapse rate (Γ) and FLH since the LGM. (**A**) Temperature versus elevation for the four lake sites (*18–20*) and the western equatorial Indian Ocean (*24*, *25*) are plotted as blue circles, and the accompanying linear regression with the 68% CI is shown as the blue line with shading (see the Supplementary Materials). The modern temperature regression and 68% CI (see the Supplementary Materials) are plotted in red for reference. (**B**) Probability distribution plots of LGM to modern elevation changes for the FLH based on GDGT temperature reconstructions (blue) and East African ELAs (*27*).

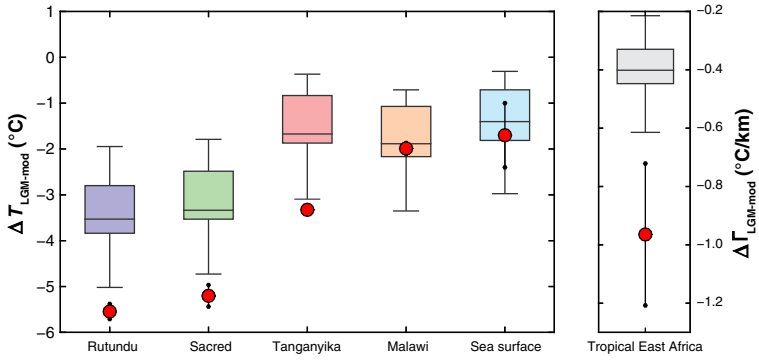

Fig. 4. Comparison of East African paleotemperature data with CMIP5/PMIP3 model output. (**A**) Site-specific temperature change (ΔT) and (**B**) lapse-rate change ($\Delta\Gamma_{LGM}$) between the LGM and PI. Red filled circles show temperature changes from GDGT proxy records, and black dots and lines mark the 1σ errors of these changes. Box and whisker plots show results from the CMIP5/PMIP3 models.

Materials). Mean tropical SST strongly influences the lapse rate and atmospheric water vapor concentrations (*29*), and $\Delta\Gamma_{LGM}$ and changes in specific humidity are correlated to the amplitude of tropical cooling in the CMIP5/PMIP3 models ($P < 0.02$ and $P < 0.04$, respectively). Although our results suggest that the models accurately simulate low-elevation temperature changes in East Africa, changes in the lapse rate are particularly sensitive to SST changes in regions of deep atmospheric convection, such as the tropical Western Pacific (*31*), where there are uncertainties in the magnitude of LGM cooling (*9*). Nevertheless, our results have potentially important implications for the equilibrium climate sensitivity (ECS) of global climate models. Atmospheric water vapor is the greatest positive feedback on global temperature, whereas the lapse rate is one of the greatest negative feedbacks (*29*). Our results suggest that both these feedbacks may be underestimated. Although model-simulated changes in lapse rate are not significantly correlated with each model's ECS, the two models with the highest ECS do simulate the largest changes in $\Delta\Gamma_{LGM}$.

CONCLUSION

Our results demonstrate that, as the world warmed from the last ice age to the Holocene, rising temperature and atmospheric humidity caused the altitudinal temperature gradient over the tropics to become less steep. State-of-the-art climate models capture the sign of this change (increase versus decrease) but underestimate its magnitude. Our data suggest that, in the tropics, this deficiency is especially marked in high-altitude areas. Thus, future anthropogenic warming on tropical mountains may be greater than current model projections indicate.

MATERIALS AND METHODS

Core collection and chronology

The Lake Rutundu temperature record (fig. S1 and table S1) was constructed using samples from two cores: Rut09, a 3.2-m-long composite core collected in 2009 from 10-m water depth using a square-rod piston corer, and Rut96, as described by Ficken *et al.* (*32*). The age model for Rut09 is based on 19 radiocarbon ages measured at 14CHRONO Centre for Climate (UBA) in Belfast, U.K., 5 radiocarbon ages measured at the National Ocean Sciences Accelerated Mass Spectrometry Facility in Woods Hole, MA, and 10 ^{210}Pb ages (fig. S2A and tables S2 and S3). The age model for Rut96 is based on 16 published radiocarbon dates (fig. S2B) (*32*). Age models were constructed with Bacon2.2 (*33*) using the Intcal13 radiocarbon curve (*34*). Three event deposits were identified in the Rut09 core (a tephra layer at 249 to 251 cm and turbidites at 254 to 256.5 cm and 312 to 314 cm), which were removed before running the Bacon2.2 software and reinserted into the final age model (fig. S2A). Total organic carbon (TOC), δ^{13}C of TOC, and magnetic susceptibility (*32*) are consistent between the two cores (fig. S2, C to E), giving us confidence in our ability to splice together the brGDGT records from both cores to create a composite temperature record spanning the last 25,000 years.

For consistency, age models for the temperature reconstructions from the other three sites were also redone using Bacon2.2 (fig. S3) (*33*). Reservoir ages and errors for Lake Tanganyika were calculated using a weighted linear regression of the logarithm of the ^{14}C offset between plant material and TOC versus ^{14}C of TOC (*35*), and the 7000-year hiatus in NP04-KH04-3A-1K was identified at 402 cm (*19*). Reservoir ages for the Lake Malawi core were considered constant (450 years) for both cores (*36*).

Lipid extraction and analysis

Samples were prepared as previously described (*20*). Briefly, 1 cm^3 of sediment was freeze-dried and homogenized. Lipids were extracted with Dionex 350 Accelerated Solvent Extractor using 1:1 (v/v) dichloromethane (DCM)/methanol (MeOH). The total lipid extract was run over an Al_2O_3 column using 9:1 hexane/DCM and 1:1 DCM/MeOH as eluents to isolate the apolar and polar fractions, respectively. Polar fractions were analyzed by atmospheric pressure chemical ionization/high-performance liquid chromatography–mass spectrometry using selective ion monitoring mode on Agilent/Hewlett-Packard 1100 Series LC/MSD with an Alltech Prevail Cyano column (150 × 2.1 mm, 3 μm).

Temperature reconstruction

The air temperature history at Lake Rutundu and Sacred Lake was reconstructed using the brGDGT calibration for East African lakes on the basis of 110 surface sediment samples (fig. S4A) (*20*). Temperatures at Lakes Tanganyika and Malawi were reconstructed on the basis of linear calibration of TEX_{86} versus temperature (fig. S4) from large lakes (*37*) and marine data excluding samples from the Red Sea (*38*). This calibration produces LGM-present temperature changes that are identical to the most recent lacustrine TEX_{86} temperature calibration (*39*) but with lower errors because of the significant increase in the number of calibration points. To account for the offset in TEX_{86} values between short cores of surface sediment and piston cores of the deeper sediments used

Downloaded from http://advances.sciencemag.org/ on April 18, 2017

to create the Lake Tanganyika temperature reconstruction (*19*), we added the average offset (0.011) to the TEX_{86} values from core NP04-KH04-4A-1K before applying the TEX_{86} calibration, as outlined above. Errors on the temperature reconstructions were calculated by bootstrapping the errors on the respective calibrations 1000 times.

Lapse rate and FLH calculations

Lapse rates were obtained by taking the slope of the linear regression of temperature versus elevation, whereas FLHs were obtained by taking the *y*-intercept of a linear regression of elevation versus temperature. Errors on lapse rates and FLHs are defined as the SEs on the respective regression coefficients. Modern lapse rates were calculated from shielded air-temperature loggers deployed on the Rwenzori Mountains, western Uganda, in combination with station data from the Global Summary of the Day data set and National Centers for Environmental Prediction/National Center for Atmospheric Research (NCEP/NCAR) reanalysis data (*40*) from the regions encompassing the Rwenzori Mountains and Mount Kenya (fig. S5). Because the free-air lapse rate from NCEP reanalysis data (−5.8°C/km) was nearly identical to the environmental lapse rate we calculated from observational data in the Rwenzori Mountains of western Uganda (−5.9°C/km), and an analysis of covariance test showed that individual regressions of these three data sets are not significantly different ($P = 0.22$), we estimated the modern regional lapse rate from all three data sets combined. Site-specific modern free-air temperatures, including that at the sea surface, were calculated from the regional lapse rate.

For each site, changes in temperature (ΔT) were calculated by subtracting the mean LGM (20.1 to 23.4 ka) temperature from mean PI era (0 to 2 ka) temperatures. This approach reduces systematic calibration error and site-specific effects because the GDGTs are likely to more accurately record the difference between LGM and recent temperature than the absolute values. Errors used in the weighted mean were calculated as bootstrapped errors on the reconstruction. Absolute LGM temperatures were calculated by subtracting ΔT from the recent (0 to 2 ka) temperatures at each site.

Both sea and lake levels changed during the LGM relative to the present, requiring that we adjust the elevation of the reconstructed LGM temperatures to estimate $\Delta\Gamma_{LGM}$. To account for lake-level change at the LGM, we lowered the elevations of Lakes Tanganyika and Malawi by 160 m (*41*) and 100 m (*42*), respectively, based on lake-level reconstructions. The sea surface was lowered by 130 m (*43*). The elevations of Lake Rutundu and Sacred Lake were considered the same as modern elevations because both lakes are very shallow (10.8 and 5.0 m, respectively).

Paleoclimate model analysis

We analyzed simulations completed for CMIP5/PMIP3 (tables S4 and S5) (*44*). These simulations were completed at varying resolutions (table S6), and their boundary conditions generally followed the PMIP3 protocols with a few exceptions. For the PI simulation, the models used atmospheric greenhouse gas concentrations at 1750 CE levels [CO_2 = 280 parts per million (ppm), CH_4 = 760 parts per billion (ppb), N_2O = 270 ppb] and orbital parameters for 1950 CE. For the LGM simulation, the models used atmospheric greenhouse gas concentrations inferred from ice cores (CO_2 = 185 ppm, CH_4 = 350 ppb, N_2O = 200 ppb) (*45–47*), 21-ka orbital parameters (*48*), and altered continental topography, land-sea mask, and ice-sheet extent based on a blended product of three different ice-sheet reconstructions (*49–51*). Exceptions to the CMIP5 boundary conditions included the ice-sheet configuration used by the Goddard Institute for Space Studies model, which is qualitatively similar to the CMIP5 blended product, and vegetation distributions that are not consistently set among the models.

Atmospheric temperature and specific humidity output from the LGM and PI experiments were averaged over 100-year output for the region covered by the GDGT temperature reconstructions (12°S to 5°N, 28°E to 40°E) from the levels of 925, 850, 700, 600, 500, 400, and 300 mbar (fig. S7). Lapse rates were calculated by regressing the annual mean temperature against elevation, which was calculated from the associated geopotential heights. Lapse rates from the PI and LGM experiments were used to calculate changes in free-air temperatures at the elevations associated with the quantitative paleotemperature reconstructions, accounting for lake- and sea-level changes outlined above. Lapse-rate changes for each model were also calculated for comparison with the observed data. To test the correlation between humidity and lapse-rate changes, we calculated the level thickness–weighted average atmospheric relative and specific humidity and conducted a two-tailed *t* test between the change in atmospheric humidity and lapse rate between the LGM and PI.

SUPPLEMENTARY MATERIALS

Supplementary material for this article is available at http://advances.sciencemag.org/cgi/content/full/3/1/e1600815/DC1

fig. S1. Lake Rutundu brGDGT-based temperature reconstruction with 68 and 95% CIs and ^{14}C age control points.

fig. S2. Age models for the Lake Rutundu cores with data supporting stratigraphic correlations between the cores.

fig. S3. Age models for cores from Sacred Lake, Lake Tanganyika, and Lake Malawi.

fig. S4. brGDGT and TEX_{86} temperature calibrations.

fig. S5. Modern elevation versus temperature data over East Africa derived from NCEP reanalysis data and temperature loggers in the Rwenzori Mountains.

fig. S6. Map showing geographic variations in the temperature lapse rate over East Africa derived from NCEP reanalysis data.

fig. S7. Correlations between changes in the lapse rate and humidity and mean tropical temperature as simulated by the CMIP5/PMIP3 models.

table S1. brGDGT temperature reconstructions from Lake Rutundu.

table S2. Radiocarbon ages used to construct an age model for the Lake Rutundu core.

table S3. ^{210}Pb data used to construct an age model for the Lake Rutundu core.

table S4. Temperatures, lapse rates, and ECSs of the CMIP5/PMIP3 climate models used in this study.

table S5. Summary information about the CMIP5/PMIP3 models used in this study.

References (*52–59*)

REFERENCES AND NOTES

1. L. G. Thompson, E. Mosley-Thompson, M. E. Davis, H. H. Brecher, Tropical glaciers, recorders and indicators of climate change, are disappearing globally. *Ann. Glaciol.* **52**, 23–34 (2011).
2. R. S. Bradley, M. Vuille, H. F. Diaz, W. Vergara, Threats to water supplies in the Tropical Andes. *Science* **312**, 1755–1756 (2006).
3. M. Collins, R. Knutti, J. Arblaster, J.-L. Dufresne, T. Fichefet, P. Friedlingstein, X. Gao, W. J. Gutowski, T. Johns, G. Krinner, M. Shongwe, C. Tebaldi, A. J. Weaver, M. Wehner, in *Climate Change 2013: The Physical Science Basis. Contribution of Working Group I to the Fifth Assessment Report of the Intergovernmental Panel on Climate Change*, T. F. Stocker, D. Qin, G.-K. Plattner, M. Tignor, S. K. Allen, J. Boschung, A. Nauels, Y. Xia, V. Bex, P. M. Midgley, Eds. (Cambridge Univ. Press, 2013), pp. 1029–1136.
4. CLIMAP Project Members, The surface of the ice-age Earth. *Science* **191**, 1131–1137 (1976).
5. P. J. Webster, N. A. Streten, Late Quaternary ice age climates of tropical Australasia: Interpretations and reconstructions. *Quat. Res.* **10**, 279–309 (1978).
6. D. Rind, D. Peteet, Terrestrial conditions at the Last Glacial Maximum and CLIMAP sea-surface temperature estimates: Are they consistent? *Quat. Res.* **24**, 1–22 (1985).
7. T. J. Crowley, Climap SSTs re-revisited. *Climate Dynam.* **16**, 241–255 (2000).
8. M. Kageyama, S. P. Harrison, A. Abe-Ouchi, The depression of tropical snowlines at the last glacial maximum: What can we learn from climate model experiments? *Quat. Int.* **138–139**, 202–219 (2005).

Downloaded from http://advances.sciencemag.org/ on April 18, 2017

9. A. K. Tripati, S. Sahany, D. Pittman, R. A. Eagle, J. D. Neelin, J. L. Mitchell, L. Beaufort, Modern and glacial tropical snowlines controlled by sea surface temperature and atmospheric mixing. *Nat. Geosci.* **7**, 205–209 (2014).
10. MARGO Project Members, Constraints on the magnitude and patterns of ocean cooling at the Last Glacial Maximum. *Nat. Geosci.* **2**, 127–132 (2009).
11. I. Farrera, S. P. Harrison, I. C. Prentice, G. Ramstein, J. Guiot, P. J. Bartlein, R. Bonnefille, M. Bush, W. Cramer, U. von Grafenstein, K. Holmgren, H. Hooghiemstra, G. Hope, D. Jolly, S.-E. Lauritzen, Y. Ono, S. Pinot, M. Stute, G. Yu, Tropical climates at the Last Glacial Maximum: A new synthesis of terrestrial palaeoclimate data. I. Vegetation, lake-levels and geochemistry. *Climate Dynam.* **15**, 823–856 (1999).
12. F. A. Street-Perrott, Palaeo-perspectives: Changes in terrestrial ecosystems. *Ambio* **23**, 37–43 (1994).
13. S. Hastenrath, Climatic forcing of glacier thinning on the mountains of equatorial East Africa. *Int. J. Climatol.* **30**, 146–152 (2010).
14. S. E. Loomis, J. M. Russell, H. Eggermont, D. Verschuren, J. S. Sinninghe Damsté, Effects of temperature, pH and nutrient concentration on branched GDGT distributions in East African lakes: Implications for paleoenvironmental reconstruction. *Org. Geochem.* **66**, 25–37 (2014).
15. S. Schouten, E. C. Hopmans, J. S. Sinninghe Damsté, The organic geochemistry of glycerol dialkyl glycerol tetraether lipids: A review. *Org. Geochem.* **54**, 19–61 (2013).
16. M. A. Berke, T. C. Johnson, J. P. Werne, S. Schouten, J. S. Sinninghe-Damsté, A mid-Holocene thermal maximum at the end of the African Humid Period. *Earth Planet. Sci. Lett.* **351–352**, 95–104 (2012).
17. M. A. Berke, T. C. Johnson, J. P. Werne, D. A. Livingstone, K. Grice, S. Schouten, J. S. Sinninghe Damsté, Characterization of the last deglacial transition in tropical East Africa: Insights from Lake Albert. *Palaeogeogr. Palaeoclimatol. Palaeoecol.* **409**, 1–8 (2014).
18. L. A. Powers, T. C. Johnson, J. P. Werne, I. S. Castañeda, E. C. Hopmans, J. S. Sinninghe Damsté, S. Schouten, Large temperature variability in the southern African tropics since the last glacial maximum. *Geophys. Res. Lett.* **32**, L08706 (2005).
19. J. E. Tierney, J. M. Russell, Y. Huang, J. S. Sinninghe Damsté, E. C. Hopmans, A. S. Cohen, Northern hemisphere controls on tropical southeast African climate during the past 60,000 years. *Science* **322**, 252–255 (2008).
20. S. E. Loomis, J. M. Russell, B. Ladd, F. A. Street-Perrott, J. S. Sinninghe Damsté, Calibration and application of the branched GDGT temperature proxy on East African lake sediments. *Earth Planet. Sci. Lett.* **357–358**, 277–288 (2012).
21. J. Tierney, J. M. Russell, Abrupt climate change in southeast tropical Africa influenced by Indian monsoon variability and ITCZ migration. *Geophys. Res. Lett.* **34**, L15709 (2007).
22. M. A. Kelly, J. M. Russell, M. B. Baber, J. A. Howley, S. E. Loomis, S. Zimmerman, B. Nakileza, J. Lukaye, Expanded glaciers during a dry and cold Last Glacial Maximum in equatorial East Africa. *Geology* **42**, 519–522 (2014).
23. R. Bonnefille, F. Chalié, J. Guiot, A. Vincens, Quantitative estimates of full glacial temperatures in equatorial Africa from palynological data. *Climate Dynam.* **6**, 251–257 (1992).
24. E. Bard, F. Rostek, C. Sonzogni, Interhemispheric synchrony of the last deglaciation inferred from alkenone paleothermometry. *Nature* **385**, 707–710 (1997).
25. C. Sonzogni, E. Bard, F. Rostek, Tropical sea-surface temperatures during the last glacial period: A view based on alkenones in Indian Ocean sediments. *Quat. Sci. Rev.* **17**, 1185–1201 (1998).
26. A. H. Sobel, J. Nilsson, L. M. Polvani, The weak temperature gradient approximation and balanced tropical moisture waves. *J. Atmos. Sci.* **58**, 3650–3665 (2001).
27. G. Kaser, H. Osmaston, *Tropical Glaciers* (Cambridge Univ. Press, 2002).
28. J. P. Peixoto, A. H. Oort, *Physics of Climate* (American Institute of Physics, 1992), 520 pp.
29. B. J. Soden, I. M. Held, An assessment of climate feedbacks in coupled ocean–atmosphere models. *J. Climate* **19**, 3354 (2006).
30. B. L. Otto-Bliesner, J. M. Russell, P. U. Clark, Z. Liu, J. T. Overpeck, B. Konecky, P. deMenocal, S. E. Nicholson, F. He, Z. Lu, Coherent changes of southeastern equatorial and northern African rainfall during the last deglaciation. *Science* **346**, 1223–1227 (2014).
31. T. J. Flannaghan, S. Fueglistaler, I. M. Held, S. Po-Chedley, B. Wyman, M. Zhao, Tropical temperature trends in atmospheric general circulation model simulations and the impact of uncertainties in observed SSTs. *J. Geophys. Res. Atmos.* **119**, 13327–13337 (2014).
32. K. J. Ficken, M. J. Wooller, D. L. Swain, F. A. Street-Perrott, G. Eglinton, Reconstruction of a subalpine grass-dominated ecosystem, Lake Rutundu, Mount Kenya: A novel multi-proxy approach. *Palaeogeogr. Palaeoclimatol. Palaeoecol.* **177**, 137–149 (2002).
33. M. Blaauw, R. Bakker, J. A. Christen, V. A. Hall, J. van der Plicht, A Bayesian framework for age modeling of radiocarbon-dated peat deposits: Case studies from the Netherlands. *Radiocarbon* **49**, 357–367 (2007).
34. P. J. Reimer, E. Bard, A. Bayliss, J. W. Beck, P. G. Blackwell, C. B. Ramsey, C. E. Buck, H. Cheng, R. L. Edwards, M. Friedrich, P. M. Grootes, T. P. Guilderson, H. Haflidason, I. Hajdas, C. Hatté, T. J. Heaton, D. L. Hoffmann, A. G. Hogg, K. A. Hughen, K. F. Kaiser, B. Kromer, S. W. Manning, M. Niu, R. W. Reimer, D. A. Richards, E. M. Scott, J. R. Southon, R. A. Staff, C. S. M. Turney, J. van der Plicht, Intcal13 and Marine13 radiocarbon age calibration curves 0–50,000 years cal BP. *Radiocarbon* **55**, 1869–1887 (2013).
35. A. A. Felton, J. M. Russell, A. S. Cohen, M. E. Baker, J. T. Chesley, M. M. McGlue, K. E. Lezzar, J. S. Pigati, J. Quade, J. C. Stager, Geochemical and sedimentological records of late Quaternary climate change, Lake Tanganyika, tropical East Africa. *Palaeogeogr. Palaeoclimatol. Palaeoecol.* **252**, 405 (2007).
36. T. C. Johnson, E. T. Brown, J. McManus, S. Barry, P. Barker, F. Gasse, A high-resolution paleoclimate record spanning the past 25,000 years in southern East Africa. *Science* **296**, 113–132 (2002).
37. L. Powers, J. P. Werne, A. J. Vanderwoude, J. S. Sinninghe Damsté, E. C. Hopmans, S. Schouten, Applicability and calibration of the TEX_{86} paleothermometer in lakes. *Org. Geochem.* **41**, 404–413 (2010).
38. J. E. Tierney, M. P. Tingley, A Bayesian, spatially-varying calibration model for the TEX_{86} proxy. *Geochim. Cosmochim. Acta* **127**, 83–106 (2014).
39. I. S. Castañeda, S. Schouten, A review of molecular organic proxies for examining modern and ancient lacustrine environments. *Quat. Sci. Rev.* **30**, 2851–2891 (2011).
40. E. Kalnay, M. Kanamitsu, R. Kistler, W. Collins, D. Deaven, L. Gandin, M. Iredell, S. Saha, G. White, J. Woollen, Y. Zhu, M. Chelliah, W. Ebisuzaki, W. Higgins, J. Janowiak, K. C. Mo, C. Ropelewski, J. Wang, A. Leetmaa, R. Reynolds, R. Jenne, D. Joseph, The NCEP/NCAR 40-year reanalysis project. *Bull. Am. Meteorol. Soc.* **77**, 437–471 (1996).
41. A. S. Cohen, K.-E. Lezzar, J.-J. Tiercelin, M. Soreghan, New palaeogeographic and lake-level reconstructions of Lake Tanganyika: Implications for tectonic, climatic, and biological evolution in a rift lake. *Basin Res.* **9**, 107–132 (1997).
42. C. A. Scholz, T. C. Johnson, A. S. Cohen, J. W. King, J. A. Peck, J. T. Overpeck, M. R. Talbot, E. T. Brown, L. Kalindekafe, P. Y. O. Amoako, R. P. Lyons, T. M. Shanahan, I. S. Castañeda, C. W. Heil, S. L. Forman, L. R. McHargue, K. R. Beuning, J. Gomez, J. Pierson, East African megadroughts between 135 and 75 thousand years ago and bearings on early-modern human origins. *Proc. Natl. Acad. Sci. U.S.A.* **104**, 16416–16421 (2007).
43. P. U. Clark, A. S. Dyke, J. D. Shakun, A. E. Carlson, J. Clark, B. Wohlfarth, J. X. Mitrovica, S. W. Hostetler, A. M. McCabe, The Last Glacial Maximum. *Science* **325**, 710–714 (2009).
44. P. Braconnot, S. P. Harrison, M. Kageyama, P. J. Bartlein, V. Masson-Delmotte, A. Abe-Ouchi, B. Otto-Bliesner, Y. Zhao, Evaluation of climate models using palaeoclimatic data. *Nat. Clim. Change* **2**, 417–424 (2012).
45. J. Flückiger, A. Dällenbach, T. Blunier, B. Stauffer, T. F. Stocker, D. Raynaud, J.-M. Barnola, Variations in atmospheric N_2O concentration during abrupt climatic changes. *Science* **285**, 227–230 (1999).
46. A. Dällenbach, T. Blunier, J. Flückiger, B. Stauffer, J. Chappellaz, D. Raynaud, Changes in the atmospheric CH_4 gradient between Greenland and Antarctica during the Last Glacial and the transition to the Holocene. *Geophys. Res. Lett.* **27**, 1005–1008 (2000).
47. E. Monnin, A. Indermühle, A. Dällenbach, J. Flückiger, B. Stauffer, T. F. Stocker, D. Raynaud, J.-M. Barnola, Atmospheric CO_2 concentrations over the last glacial termination. *Science* **291**, 112–114 (2001).
48. A. L. Berger, Long-term variations of caloric insolation resulting from the Earth's orbital elements. *Quat. Res.* **9**, 139–167 (1978).
49. D. F. Argus, W. R. Peltier, Constraining models of postglacial rebound using space geodesy: A detailed assessment of model ICE-5G (VM2) and its relatives. *Geophys. J. Int.* **181**, 697–723 (2010).
50. L. Tarasov, W. R. Peltier, A geophysically constrained large ensemble analysis of the deglacial history of the North American ice-sheet complex. *Quat. Sci. Rev.* **23**, 359–388 (2004).
51. K. Lambeck, A. Purcell, J. Zhao, N.-O. Svensson, The Scandinavian Ice Sheet: From MIS 4 to the end of the Last Glacial Maximum. *Boreas* **39**, 410–435 (2010).
52. P. O. Hopcroft, P. J. Valdes, How well do simulated last glacial maximum tropical temperatures constrain equilibrium climate sensitivity? *Geophys. Res. Lett.* **42**, 5533–5539 (2015).
53. E. C. Brady, B. L. Otto-Bliesner, J. E. Kay, N. Rosenbloom, Sensitivity to glacial forcing in the CCSM4. *J. Climate* **26**, 1901–1925 (2013).
54. A. Voldoire, E. Sanchez-Gomez, D. Salas y Mélia, B. Decharme, C. Cassou, S. Sénési, S. Valcke, I. Beau, A. Alias, M. Chevallier, M. Déqué, J. Deshayes, H. Douville, E. Fernandez, G. Madec, E. Maisonnave, M.-P. Moine, S. Planton, D. Saint-Martin, S. Szopa, S. Tyteca, R. Alkama, S. Belamari, A. Braun, L. Coquart, F. Chauvin, The CNRM-CM5.1 global climate model: Description and basic evaluation. *Climate Dynam.* **40**, 2091–2121 (2013).
55. D. J. Ullman, A. N. LeGrande, A. E. Carlson, F. S. Anslow, J. M. Licciardi, Assessing the impact of Laurentide Ice Sheet topography on glacial climate. *Clim. Past Discuss.* **9**, 3239–3306 (2013).
56. M. Kageyama, P. Braconnot, L. Bopp, A. Caubel, M.-A. Foujols, E. Guilyardi, M. Khodri, J. Lloyd, F. Lombard, V. Mariotti, O. Marti, T. Roy, M.-N. Woillez, Mid-Holocene and Last Glacial Maximum climate simulations with the IPSL model—Part I: Comparing IPSL_CM5A to IPSL_CM4. *Climate Dynam.* **40**, 2447–2468 (2013).
57. S. Watanabe, T. Hajima, K. Sudo, T. Nagashima, T. Takemura, H. Okajima, T. Nozawa, H. Kawase, M. Abe, T. Yokohata, T. Ise, H. Sato, E. Kato, K. Takata, S. Emori, M. Kawamiya, MIROC-ESM 2010: Model description and basic results of CMIP5-20c3m experiments. *Geosci. Model Dev.* **4**, 845–872 (2011).

Downloaded from http://advances.sciencemag.org/ on April 18, 2017

58. T. Mauritsen, B. Stevens, E. Roeckner, T. Crueger, M. Esch, M. Giorgetta, H. Haak, J. Jungclaus, D. Klocke, D. Matei, U. Mikolajewicz, D. Notz, R. Pincus, H. Schmidt, L. Tomassini, Tuning the climate of a global model. *J. Adv. Model. Earth Syst.* **4**, M00A01 (2012).
59. S. Yukimoto, Y. Adachi, M. Hosaka, T. Sakami, H. Yoshimura, M. Hirabara, T. Y. Tanaka, E. Shindo, H. Tsujino, M. Deushi, R. Mizuta, S. Yabu, A. Obata, H. Nakano, T. Koshiro, T. Ose, A. Kitoh, A new global climate model of the Meteorological Research Institute: MRI-CGCM3—Model description and basic performance. *J. Meteorol. Soc. Jpn.* **90A**, 23–64 (2012).

Acknowledgments: We thank A. Heureux, L. Messier, and R. Tarozo for assistance in the laboratory; B. Konecky and T. Shanahan for helpful discussions; and Ngaara Mountaineering Services, the Kenya Wildlife Service, S. M. Rucina (National Museums of Kenya), and the University of Nairobi (D. O. Olago) for logistical support. We acknowledge the World Climate Research Program's Working Group on Coupled Modeling, which is responsible for CMIP, and the individual modeling groups for producing and sharing model output. **Funding:** This work was conducted with funds from the NSF under grant number EAR-1226566 to J.M.R. and by a Geological Society of America Graduate Student Research Grant awarded to S.E.L. The Rutundu core Rut06 was collected by the late R. A. Perrott, with permission from the Office of the President, Nairobi (OP/13/001/25C). Fieldwork was supported by U.K. Natural Environment Research Council grant GR3/9523 and 14C Dating Allocation 708/0997. Collection of Rutundu core Rut09 was sponsored by the Fund of Scientific Research of Flanders (FWO-Vlaanderen) and conducted with permits from the National Council for Science and Technology of Kenya (NCST/5/002/R/439/4), Kenya Wildlife Service (KWS/CL&P/029), and National Environmental Monitoring Authority (NEMA Access Permit AGR/7/2010). It was exported under material transfer agreement A11/TT/1040 between the Kenya Wildlife Service, the University of Nairobi, and Ghent University. J.S.S.D. is supported by the Netherlands Earth System Science Center through a gravitation grant from the Dutch Ministry for Education, Culture, and Science (024.002.001). **Author contributions:** J.M.R. and S.E.L. designed the study. D.V., H.E., G.D.C., F.A.S.-P., and D.O. provided sediment core samples and corollary data. S.E.L. performed the laboratory and instrumental analyses and conducted statistical analyses of the data. C.M. analyzed climate model output. All authors contributed to the interpretation of the data. J.M.R. and S.E.L. wrote the manuscript together with all coauthors. **Competing interests:** The authors declare that they have no competing interests. **Data and materials availability:** All data needed to evaluate the conclusions in the paper are present in the paper and/or the Supplementary Materials and in the World Data Center A for Paleoclimatology. Additional data related to this paper may be requested from the authors.

Submitted 18 April 2016
Accepted 19 December 2016
Published 27 January 2017
10.1126/sciadv.1600815

Citation: S. E. Loomis, J. M. Russell, D. Verschuren, C. Morrill, G. De Cort, J. S. Sinninghe Damsté, D. Olago, H. Eggermont, F. A. Street-Perrott, M. A. Kelly, The tropical lapse rate steepened during the Last Glacial Maximum. *Sci. Adv.* **3**, e1600815 (2017).

Downloaded from http://advances.sciencemag.org/ on April 18, 2017

Science Advances

The tropical lapse rate steepened during the Last Glacial Maximum

Shannon E. Loomis, James M. Russell, Dirk Verschuren, Carrie Morrill, Gijs De Cort, Jaap S. Sinninghe Damsté, Daniel Olago, Hilde Eggermont, F. Alayne Street-Perrott and Meredith A. Kelly

(January 27, 2017)
Sci Adv 2017, 3:.
doi: 10.1126/sciadv.1600815

This article is publisher under a Creative Commons license. The specific license under which this article is published is noted on the first page.

For articles published under CC BY licenses, you may freely distribute, adapt, or reuse the article, including for commercial purposes, provided you give proper attribution.

For articles published under CC BY-NC licenses, you may distribute, adapt, or reuse the article for non-commerical purposes. Commercial use requires prior permission from the American Association for the Advancement of Science (AAAS). You may request permission by clicking here.

The following resources related to this article are available online at http://advances.sciencemag.org. (This information is current as of April 18, 2017):

Updated information and services, including high-resolution figures, can be found in the online version of this article at:
http://advances.sciencemag.org/content/3/1/e1600815.full

Supporting Online Material can be found at:
http://advances.sciencemag.org/content/suppl/2017/01/23/3.1.e1600815.DC1

This article **cites 56 articles,** 11 of which you can access for free at:
http://advances.sciencemag.org/content/3/1/e1600815#BIBL

Science Advances (ISSN 2375-2548) publishes new articles weekly. The journal is published by the American Association for the Advancement of Science (AAAS), 1200 New York Avenue NW, Washington, DC 20005. Copyright is held by the Authors unless stated otherwise. AAAS is the exclusive licensee. The title Science Advances is a registered trademark of AAAS

Downloaded from http://advances.sciencemag.org/ on April 18, 2017